Two-Dimensional Prony Modeling and Parameter Estimation

Joseph J. Sacchini, *Member, IEEE,* William M. Steedly, *Member, IEEE,* and Randolph L. Moses, *Senior Member, IEEE*

***Abstract*—A new method for estimating the two-dimensional (2-D) exponential modes and amplitude coefficients in a Prony model is presented. This method involves two parts, each utilizing a 1-D singular value decomposition-based technique, and is capable of locating frequencies anywhere in the 2-D frequency plane. Simulations are shown which demonstrate the performance of the algorithm.**

I. Introduction

FOR many years the problem of two-dimensional (2-D) frequency and amplitude coefficient estimation from a 2-D data set has been investigated. This problem has applications in sonar, radar, geophysics, radio astronomy, radio communications, and medical imaging [1]–[7]. Many techniques have been applied to the problem such as Fourier-based methods, data extension, maximum likelihood method (MLM), maximum entropy method (MEM), autoregressive (AR) models, and linear prediction (LP) models [8]–[15].

Fourier-based methods are currently used in tomography to generate an image of an object [2]–[6]. The properties of these techniques have been well studied [2]. However, these techniques are limited by Fourier resolution capabilities. Also, these techniques do not directly estimate the frequencies. Thresholding must be used in the 2-D frequency domain to determine the frequencies.

Other methods include the MLM of spectral estimation which was proposed as an m-dimensional (m-D) technique for array processing [8]. This technique has also been applied to the tomography problem in [14]. The MEM of spectral estimation has also been applied to the 2-D problem [10], [11], [15]. This method also provides high resolution, but does not exist for all data sets [16]. Two-dimensional AR modeling and algorithms exist [9], [12], [13], as well as state space methods [17]. A matrix pencil method [18] has also been used.

Prony's method coupled with total least squares (TLS) techniques in one-dimension (1-D) has been used successfully to estimate frequencies in the presence of noise [19]. For the 2-D problem, an iterative constrained total least squares (CTLS) algorithm has been applied to provide frequencies [20]. In this paper, 2-D frequencies and amplitude coefficients are estimated by a noniterative two-step method using a 1-D TLS-based Prony model and estimation technique in each step. This method is capable of locating frequencies anywhere in the 2-D plane, along with their damping factors.

A related method, developed by Hua [18], also estimates 2-D frequencies. In Hua's method, two estimation steps are performed to separately estimate the x-components and y-components of the 2-D frequencies. Then, a matching step is performed to find the correct x-component and y-component frequency pairings. The method we present is similar to Hua's in some respects, but different in others. First, we estimate the x-components of the frequencies. Then, we use the amplitude coefficients corresponding to each x-component frequency to estimate a set of y-components. In this way, we avoid the requirement of a matching step. Our algorithm is computationally less expensive than Hua's method, and more amenable to parallel implementation. We also present a second algorithm in which the first algorithm is used twice, first to estimate x then y-components and then y then x-components. This second algorithm does require matching, but gives more accurate parameter estimates than does the first method. Both methods we present have a smaller computational load than Hua's method, but Hua's method generally gives more accurate parameter estimates. Thus, the methods we present are lower computational alternatives to [18], for cases in which some loss in accuracy can be tolerated.

An outline of this paper is as follows. In Section II, the data model and parameter estimation procedures are presented, along with computational issues. Section III presents simulations using the estimation procedure. Finally, Section IV concludes the paper.

Manuscript received January 14, 1992; revised August 19, 1992. The associate editor coordinating the review of this paper and approving it for publication was Prof. Russell M. Mersereau.

This work was supported in part by the Air Force Office of Scientific Research, Bolling Air Force Base, DC and in part by the Avionics Division, Wright Laboratories, Wright Patterson Air Force Base, OH.

J. J. Sacchini is with the Department of Electrical and Computer Engineering, Air Force Institute of Technology, Wright Patterson Air Force Base, OH 45433.

W. M. Steedly is with The Analytic Sciences Corporation (TASC), Reston, VA 22090.

R. L. Moses is with the Department of Electrical Engineering, Ohio State University, Columbus, OH 43210.

IEEE Log Number 9211542.

II. Data Model and Estimation Algorithms

A. Data Model

It is assumed that we are given noisy 2-D data which has the form

$$d'(m, n) = d(m, n) + w(m, n), \tag{1}$$

where $m = 0, 1, \cdots, M-1$ and $n = 0, 1, \cdots, N-1$ and $w(m, n)$ is 2-D noise sequence. We will refer to the first index of $d(m, n)$ as the x-component, and the second index as the y-component.

The noiseless data is assumed to fit the damped exponential model

$$d(m, n) = \sum_{k=1}^{K} \sum_{l=1}^{L_k} a_{k,l} p_{x_k}^m p_{y_{k,l}}^n, \tag{2}$$

where

$$\begin{aligned} p_{x_k} &= k\text{th } x\text{-pole, } x\text{-component of 2-D exponential} \\ p_{y_{k,l}} &= k, l\text{th } y\text{-pole, } y\text{-component of 2-D exponential} \\ a_{k,l} &= k, l\text{th amplitude coefficient} \\ L_k &= \text{number of } y\text{-poles corresponding to the } k\text{th } x\text{-pole.} \end{aligned} \tag{3}$$

This model has application in 2-D frequency estimation for various applications, as well as 2-D scattering center estimation for the radar problem [21].

Given noisy data $d'(m, n)$, $n = 0, 1, \cdots, M-1$ and $n = 0, 1, \cdots, N-1$, we wish to estimate the parameters in the model (2). Below we present two TLS-based algorithms for estimating these parameters, Algorithm One and Algorithm Two.

B. Algorithm One

Algorithm One consists of four steps. The x-poles, $\{p_{x_k}\}_{k=1}^{K}$, are first estimated using a TLS-Prony algorithm. Second, a set of amplitude coefficients corresponding to these x-pole estimates are computed. The amplitude coefficients are themselves used in a set of second TLS-Prony estimates to obtain the y-pole estimates, $\{p_{y_{k,l}}\}_{l=1}^{L_k}$, which is the third step. Finally, a least squares technique is used to estimate the amplitude coefficients $\{a_{k,l}\}$. These steps are detailed below and summarized in Table I.

Step 1: Estimation of the x-poles. The first step in the parameter estimation problem is to estimate the x-poles, $\{p_{x_k}\}_{k=1}^{K}$. We now define a matrix composed of the noisy data, $\{d'(m, n)\}_{m,n=0}^{M-1,N-1}$, as

$$D' = \begin{bmatrix} d'(0,0) & d'(1,0) & \cdots & d'(M-1,0) \\ d'(0,1) & d'(1,1) & \cdots & d'(M-1,1) \\ \vdots & \vdots & & \vdots \\ d'(0,N-1) & d'(1,N-1) & \cdots & d'(M-1,N-1) \end{bmatrix}. \tag{4}$$

Each row of D' can be used to provide an estimate of the x-poles. However, in order to utilize 1-D Prony estimation procedures, all of the rows of D' will be used simultaneously in the estimation of the x-poles. A total least squares (TLS) backward linear prediction approach similar to [19] is used. The backward linear prediction equations are

$$\begin{bmatrix} d'(0,0) & d'(1,0) & d'(2,0) & \cdots & d'(Q,0) \\ d'(1,0) & d'(2,0) & d'(3,0) & \cdots & d'(Q+1,0) \\ \vdots & \vdots & \vdots & & \vdots \\ d'(M-Q-1,0) & d'(M-Q,0) & d'(M-Q+1,0) & \cdots & d'(M-1,0) \\ \hline d'(0,1) & d'(1,1) & d'(2,1) & \cdots & d'(Q,1) \\ d'(1,1) & d'(2,1) & d'(3,1) & \cdots & d'(Q+1,1) \\ \vdots & \vdots & \vdots & & \vdots \\ d'(M-Q-1,1) & d'(M-Q,1) & d'(M-Q+1,1) & \cdots & d'(M-1,1) \\ \hline & & \vdots & & \\ \hline d'(0,N-1) & d'(1,N-1) & d'(2,N-1) & \cdots & d'(Q,N-1) \\ d'(1,N-1) & d'(2,N-1) & d'(3,N-1) & \cdots & d'(Q+1,N-1) \\ \vdots & \vdots & \vdots & & \vdots \\ d'(M-Q-1,N-1) & d'(M-Q,N-1) & d'(M-Q+1,N-1) & \cdots & d'(M-1,N-1) \end{bmatrix} \begin{bmatrix} 1 \\ b_1 \\ b_2 \\ \vdots \\ b_Q \end{bmatrix} \approx 0. \tag{5}$$

TABLE I
SUMMARY OF STEPS PERFORMED IN ALGORITHM ONE

Step	Estimated Parameters	Method of Solution
1	$\{p_{x_k}\}_{k=1}^{K}$ (x-poles)	TLS of Eq. (6) w/ SVD truncation
2	$\{c_{q,n}\}_{q,n=1,0}^{Q,N-1}$ (x-amplitude coefficients)	LS of Eq. (11) via QR decomposition
3	$\{p_{y_{k,l}}\}_{k,l=1,1}^{K,L_k}$ (y-poles)	TLS of Eq. (15) w/ SVD truncation
4	$\{a_{k,l}\}_{k,l=1,1}^{K,L_k}$ (amplitude coefficients)	LS of Eq. (19) via QR decomposition

or

$$S\begin{bmatrix}1\\ b\end{bmatrix} \approx 0 \tag{6}$$

where Q is the order of prediction, and b is the coefficient vector of the polynomial $B(z)$ given by

$$B(z) = 1 + b_1 z + b_2 z^2 + \cdots + b_Q z^Q. \tag{7}$$

Ideally, Q can be any integer greater than or equal to the model order K; in practice, choosing $Q > K$ results in more accurate parameter estimates [22]–[24]. Note that all of the rows of D' are used simultaneously to estimate a single set of prediction coefficients (and therefore, a single set of x-poles).

Equation (6) is used to solve for the estimate of b, $\hat{b}$, in a total least squares sense to arrive at a minimum norm (TLS) estimate, where the $Q + 1 - K$ smallest singular values of S are truncated to arrive at a noise cleaned estimate $\hat{S}$ (see [19] for details).

The estimated x-poles are found by

$$\hat{p}_{x_q} = \text{zero}_q(\hat{B}(z)), \qquad q = 1, 2, \cdots, Q. \tag{8}$$

Because only K singular values of $\hat{S}$ are nonzero, there are at most K x-pole estimates which can correspond to data modes. Therefore, only the K x-poles which have the largest energy are retained (as discussed in Step 2 below).

Step 2: Estimation of the x-amplitude Coefficients. Before we find the y-poles we must first estimate x-amplitude coefficients. These are defined as follows:

$$c_{q,n} = \sum_{l=1}^{L_k} a_{q,l} p_{y_{q,l}}^{n}, \qquad q = 1, 2, \cdots, Q. \tag{9}$$

With this definition, the model associated with (2) using the estimated x-poles is written as

$$d(m, n) = \sum_{q=1}^{Q} c_{q,n} p_{x_q}^{m} \tag{10}$$

where $c_{q,n}$ is the qth x-amplitude coefficient associated with the nth row of D'.

Note that the equations in (10) are uncoupled for different values of n. Thus, each row of D' will give an x-amplitude coefficient estimate for each x-pole. These estimates serve as the inputs to the second Prony model and determine the y-poles. The x-amplitude coefficients are an intermediate step in the estimation procedure and are completely defined in (9). Also, note that the y-pole model orders, $\{L_k\}_{k=1}^{K}$, may be different for each of the K x-poles. Equation (10) is used to solve for the $c_{q,n}$s as follows

$$\begin{bmatrix} 1 & 1 & \cdots & 1 \\ p_{x_1} & p_{x_2} & \cdots & p_{x_Q} \\ p_{x_1}^2 & p_{x_2}^2 & \cdots & p_{x_Q}^2 \\ \vdots & \vdots & & \vdots \\ p_{x_1}^{M-1} & p_{x_2}^{M-1} & \cdots & p_{x_Q}^{M-1} \end{bmatrix} \cdot \begin{bmatrix} c_{1,0} & c_{1,1} & \cdots & c_{1,N-1} \\ c_{2,0} & c_{2,1} & \cdots & c_{2,N-1} \\ \vdots & \vdots & & \vdots \\ c_{Q,0} & c_{Q,1} & \cdots & c_{Q,N-1} \end{bmatrix} = D'^{T}. \tag{11}$$

or

$$P_x C = D'^{T}. \tag{12}$$

The x-amplitude coefficients are found from a least squares solution to (12) using the x-pole estimates, this can be written as

$$\hat{C} = (\hat{P}_x^H \hat{P}_x)^{-1} \hat{P}_x^H D'^{T}, \tag{13}$$

although numerically more robust solutions (using, e.g., the QR decomposition [25]) are preferred to direct computation of (13).

Because only K singular values of $\hat{S}$ are nonzero, there are at most K x-pole estimates which can correspond to data modes. Therefore, only the K x-poles which have the largest energy are retained. This is done by computing the Q x-mode energies as

$$E_q = \sum_{n=0}^{N-1} |\hat{c}_{q,n}|^2 \sum_{m=0}^{M-1} |\hat{p}_{x_q}|^{2m} \qquad q = 1, 2, \cdots, Q \tag{14}$$

and retaining those K poles whose corresponding energies are highest.

Step 3: Estimation of the y-poles. The x-amplitude coefficients can also be used to solve for the y-poles. For each of the K high energy x-poles, the backward linear prediction equations for the model given by (9) become

$$\begin{bmatrix} c_{k,0} & c_{k,1} & \cdots & c_{k,R_k} \\ c_{k,1} & c_{k,2} & \cdots & c_{k,R_k+1} \\ \vdots & \vdots & & \vdots \\ c_{k,N-R_k-1} & c_{k,N-R_k} & \cdots & c_{k,N-1} \end{bmatrix} \begin{bmatrix} 1 \\ b_1^k \\ b_2^k \\ \vdots \\ b_{R_k}^k \end{bmatrix} \approx 0$$

$$k = 1, 2, \cdots, K \tag{15}$$

or

$$F^k \begin{bmatrix} 1 \\ b^k \end{bmatrix} \approx 0 \tag{16}$$

where R_k is the order of prediction for the y-poles, and b^k is the coefficient vector of the polynomial $B^k(z)$ given by

$$B^k(z) = 1 + b_1^k z + b_2^k z^2 + \cdots + b_{R_k}^k z^{R_k}. \tag{17}$$

Again, R_k can be any integer greater than or equal to L_k, while in practice choosing $R_k > L_k$ results in more accurate parameter estimates [22]–[24].

Equation (16) is used to solve for the estimate of b^k, $\widehat{b^k}$, in a total least squares sense to arrive at a minimum norm (TLS) estimate, where the $R_k + 1 - L_k$ singular values of S are truncated to arrive at a noise cleaned estimate $\widehat{F^k}$ (see [19] for details).

The y-pole estimates are thus given by

$$\hat{p}_{y_{k,r_k}} = \text{zero}_{r_k}(\widehat{B^k}(z)), \qquad r_k = 1, 2, \cdots, R_k. \tag{18}$$

The procedure from (15)–(18) is carried out K times to estimate the y-poles corresponding to each of the K x-poles. Because only L_k singular values of $\widehat{F^k}$ are nonzero, there are at most L_k y-pole estimates which can correspond to data modes. Therefore, only the L_y y-poles which have the largest energy are retained (as discussed in Step 4 below).

Step 4: Estimation of the Amplitude Coefficients. Now that all of the required y-poles have been estimated, the amplitude coefficients will be estimated next. Using (9), we can write

$$\begin{bmatrix} 1 & 1 & \cdots & 1 \\ p_{y_{k,1}} & p_{y_{k,2}} & \cdots & p_{y_{k,R_k}} \\ p_{y_{k,1}}^2 & p_{y_{k,2}}^2 & \cdots & p_{y_{k,R_k}}^2 \\ \vdots & \vdots & & \vdots \\ p_{y_{k,1}}^{N-1} & p_{y_{k,2}}^{N-1} & \cdots & p_{y_{k,R_k}}^{N-1} \end{bmatrix} \begin{bmatrix} a_{k,1} \\ a_{k,2} \\ \vdots \\ a_{k,R_k} \end{bmatrix} = \begin{bmatrix} c_{k,0} \\ c_{k,1} \\ \vdots \\ c_{k,N-1} \end{bmatrix} \tag{19}$$

or

$$P_y^k A^k = c^k. \tag{20}$$

The amplitude coefficients are found from a least squares solution to (20) using the y-pole estimates along the x-amplitude coefficients; this can be written as

$$\widehat{A^k} = (\widehat{P_y^k}^H \widehat{P_y^k})^{-1} \widehat{P_y^k}^H \widehat{c^k}, \tag{21}$$

although numerically more robust solutions (using, e.g., the QR decomposition [25]) are preferred to direct computation of (21).

Because only L_k singular values of $\widehat{F^k}$ are nonzero, there are at most L_k y-pole estimates which can correspond to data modes. Therefore, only the L_k y-poles which have the largest energy are retained. This is done by computing the R_k y-mode energies for each of the kth x-poles as

$$E_{r_k} = |\hat{a}_{k,r_k}|^2 \sum_{n=0}^{N-1} |\hat{p}_{y_{k,r_k}}|^{2n} \qquad r_k = 1, 2, \cdots, R_k \tag{22}$$

TABLE II
SUMMARY OF STEPS PERFORMED IN ALGORITHM TWO

Step	Estimated Parameters	Method of Solution
1	$\{p_{x_k}\}_{k=1}^{K}$ (x-poles)	TLS of Eq. (6) w/ SVD truncation
2	$\{c_{q,n}\}_{q,n=1,0}^{Q,N-1}$ (x-amplitude coefficients)	LS of Eq. (11) via QR decomposition
3	$\{p_{y_{k,l}}\}_{k,l=1,1}^{K,L_k}$ (y-poles)	TLS of Eq. (15) w/ SVD truncation
4	$\{p_{x_{k'}}^t\}_{k'=1}^{K^t}$ (x^t-poles)	TLS similar to Step 1
5	$\{c_{q',m}^t\}_{q',m=1,0}^{Q,M-1}$ (x^t-amplitude coefficients)	LS similar to Step 2
6	$\{p_{y_{k',l'}}^t\}_{k',l'=1,1}^{K',L_{k'}^t}$ (y^t-poles)	TLS similar to Step 3
7	$\{\rho_{x_\gamma}, \rho_{y_\gamma}\}_{\gamma=1}^{\Gamma}$ (x and y-poles)	Matching using Eq. (23)
8	$\{\alpha_\gamma\}_{\gamma=1}^{\Gamma}$ (amplitude coefficients)	LS of Eq. (25) via QR decomposition

and retaining those L_k poles whose corresponding energies are highest.

C. Algorithm Two

Algorithm Two utilizes the first three steps of Algorithm One twice, and then requires a matching step and a final amplitude coefficient calculation step. The steps involved in Algorithm Two are summarized in Table II. The first three steps of Algorithm One are carried out using the data $d'(m, n)$ yielding x and y-pole estimates, $\{p_{x_k}\}_{k=1}^{K}$ and $\{p_{y_{k,l}}\}_{l=1}^{L_k}$. Next, the data is transposed [i.e., $d''(n, m) = d'(m, n)$], and Algorithm One is applied to $d''(n, m)$ to arrive at a second set of poles, $\{p_{x_{k'}}^t\}_{k'=1}^{K'}$ and $\{p_{y_{k',l'}}^t\}_{l'=1}^{L_{k'}^t}$. Note that the model orders K and L_k are related to K^t and $L_{k'}^t$, depending on the structure of a particular model, and are in general different.

The two sets of estimates are combined, and the more accurate part of the estimates from each set is retained. The more accurate part of each estimate is the set of poles which were estimated first, (i.e., the x-poles from each set). The y-poles are less accurate than the x-poles because they are estimates based on the x-pole estimates. A matching algorithm is used to combine both sets of pole estimates yielding a single set of pole estimates.

The matching is performed using the following metric:

$$\Delta((p_{x_k}, p_{y_{k,l}}), (p_{x_k}^t, p_{y_{k',l'}}^t, p_{y_{k',l'}}^t)) = \sqrt{|p_{x_k} - p_{y_{k',l'}}^t|^2 + |p_{y_{k,l}} - p_{x_{k'}}^t|^2} \tag{23}$$

for the distance between 2-D exponential modes $(p_{x_k}, p_{y_{k,l}})$ and $(p_{x_{k'}}^t, p_{y_{k',l'}}^t)$, estimated from the two estimates in Step 1. These distances are calculated for all of the possible pairs. Then the closest match is made and the respective pole pairs and distances are eliminated from consideration. The next-to-closest match is then made in the same fashion and so on, until there are no modes remaining from one of the two sets of pole pairs parts (any leftover pole pairs are discarded). Note that the x-poles, p_{x_k} and $p_{x_{k'}}^t$, from each of the two estimations are retained and the y-poles are discarded as discussed above. Thus, the y-poles are only necessary for the pairing performed in the matching step. Note that the $p_{x_{k'}}^t$ take on the role of y-poles in the original model. The final set of matched pole pairs for Algorithm Two are thus designated $\{\rho_{x_\gamma}$,

$\rho_{y_\gamma}\}_{\gamma=1}^{\Gamma}$, where the ρ's are given by the paired p_x's and p_x^t's and $\Gamma = \min\{\Sigma_{k=1}^{K} L_k, \Sigma_{k^t=1}^{K^t} L_{k^t}^k\}$.

Using this definition, the model in (2) can be expressed as

$$d(m, n) = \sum_{\gamma=1}^{\Gamma} \alpha_\gamma \rho_{x_\gamma}^m \rho_{y_\gamma}^n. \tag{24}$$

Equation (24) now is used to solve for amplitude coefficients, $\{\alpha_\gamma\}_{\gamma=1}^{\Gamma}$, as follows:

$$\begin{bmatrix}
1 & 1 & \cdots & 1 \\
\rho_{y_1} & \rho_{y_2} & \cdots & \rho_{y_\Gamma} \\
\rho_{y_1}^2 & \rho_{y_2}^2 & \cdots & \rho_{y_\Gamma}^2 \\
\vdots & \vdots & & \vdots \\
\rho_{y_1}^{N-1} & \rho_{y_2}^{N-1} & \cdots & \rho_{y_\Gamma}^{N-1} \\
\hline
\rho_{x_1} & \rho_{x_2} & \cdots & \rho_{x_\Gamma} \\
\rho_{x_1}\rho_{y_1} & \rho_{x_2}\rho_{y_2} & \cdots & \rho_{x_\Gamma}\rho_{y_\Gamma} \\
\rho_{x_1}\rho_{y_1}^2 & \rho_{x_2}\rho_{y_2}^2 & \cdots & \rho_{x_\Gamma}\rho_{y_\Gamma}^2 \\
\vdots & \vdots & & \vdots \\
\rho_{x_1}\rho_{y_1}^{N-1} & \rho_{x_2}\rho_{y_2}^{N-1} & \cdots & \rho_{x_\Gamma}\rho_{y_\Gamma}^{N-1} \\
\hline
\rho_{x_1}^2 & \rho_{x_2}^2 & \cdots & \rho_{x_\Gamma}^2 \\
\rho_{x_1}^2\rho_{y_1} & \rho_{x_2}^2\rho_{y_2} & \cdots & \rho_{x_\Gamma}^2\rho_{y_\Gamma} \\
\rho_{x_1}^2\rho_{y_1}^2 & \rho_{x_2}^2\rho_{y_2}^2 & \cdots & \rho_{x_\Gamma}^2\rho_{y_\Gamma}^2 \\
\vdots & \vdots & & \vdots \\
\rho_{x_1}^2\rho_{y_1}^{N-1} & \rho_{x_2}^2\rho_{y_2}^{N-1} & \cdots & \rho_{x_\Gamma}^2\rho_{y_\Gamma}^{N-1} \\
\hline
 & \vdots & & \\
\hline
\rho_{x_1}^{M-1}\rho_{y_1} & \rho_{x_2}^{M-1} & \cdots & \rho_{x_\Gamma}^{M-1} \\
\rho_{x_1}^{M-1} & \rho_{x_2}^{M-1}\rho_{y_2} & \cdots & \rho_{x_\Gamma}^{M-1}\rho_{y_\Gamma} \\
\rho_{x_1}^{M-1}\rho_{y_1}^2 & \rho_{x_2}^{M-1}\rho_{y_2}^2 & \cdots & \rho_{x_\Gamma}^{M-1}\rho_{y_\Gamma}^2 \\
\vdots & \vdots & & \vdots \\
\rho_{x_1}^{M-1}\rho_{y_1}^{N-1} & \rho_{x_2}^{M-1}\rho_{y_2}^{N-1} & \cdots & \rho_{x_\Gamma}^{M-1}\rho_{y_\Gamma}^{N-1}
\end{bmatrix}
\begin{bmatrix} \alpha_1 \\ \alpha_2 \\ \vdots \\ \alpha_\Gamma \end{bmatrix} =
\begin{bmatrix}
d'(0, 0) \\ d'(0, 1) \\ d'(0, 2) \\ \vdots \\ d'(0, N-1) \\
\hline
d'(1, 0) \\ d'(1, 1) \\ d'(1, 2) \\ \vdots \\ d'(1, N-1) \\
\hline
d'(2, 0) \\ d'(2, 1) \\ d'(2, 2) \\ \vdots \\ d'(2, N-1) \\
\hline
\vdots \\
\hline
d'(M-1, 0) \\ d'(M-1, 1) \\ d'(M-1, 2) \\ \vdots \\ d'(M-1, N-1)
\end{bmatrix} \tag{25}$$

or

$$\mathcal{P}\mathcal{A} = \mathcal{D}'. \tag{26}$$

The amplitude coefficients are found using the pole estimates from a least squares solution to (26) which can be written as

$$\hat{\mathcal{A}} = (\hat{\mathcal{P}}^H\hat{\mathcal{P}})^{-1}\hat{\mathcal{P}}^H\mathcal{D}', \tag{27}$$

although numerically more robust solutions (using, e.g., the QR decomposition [25]) are preferred to direct computation of (27).

D. Implementation Issues

In this subsection, we present operation counts for the four steps of Algorithm One and for the eight steps of Algorithm Two. These operation counts are given for the case when the data are real. For complex data considered in the examples below the counts were observed to be about a factor of two to three larger for the SVD's and about four times larger for the QR decompositions. We also present an alternative to the larger SVD steps which provides a reduction in computation.

1) Operation Count for Algorithm One

To obtain the operation counts for the four steps of Algorithm One, we need counts for the SVD computations and the computation of the QR decompositions used for the least squares solutions.

The approximate floating point operation (flop) count, fc_{SVD}, associated with the computation of the singular values and left singular vectors of a real $r \times c$ matrix is given by $\text{fc}_{\text{SVD}} \approx 4rc^2 + 8c^3$ [25]. Thus the flop count for the

SVD of Step 1, fc^1_{One}, is given by

$$fc^1_{One} \approx 4N(M - Q)(Q + 1)^2 + 8(Q + 1)^3. \quad (28)$$

The approximate flop count, fc_{QR}, associated with the QR decomposition of a real $r \times c$ matrix is given by $fc_{QR} \approx 2rc^2 - (2/3)c^3$ [25]. Thus, the flop count for the QR decomposition required for the LS solution of Step 2 is given by

$$fc^2_{One} \approx 2MQ^2 - \tfrac{2}{3} Q^3. \quad (29)$$

For the K SVD's, in Step 3 the approximate flop count is given by

$$fc^3_{One} \approx \sum_{k=1}^{K} (4(N - R_k)(R_k + 1)^2 + 8(R_k + 1)^3). \quad (30)$$

For the K QR decompositions in Step 4 the approximate flop count is given by

$$fc^4_{One} \approx \sum_{k=1}^{K} (2NR_k^2 - \tfrac{2}{3} R_k^3). \quad (31)$$

The flop count for the SVD's and QR decompositions of Algorithm One is given by the sum of the individual flop counts above.

To achieve near optimal performance (with respect to the CRB), the model order used for Steps 1 and 3 of Algorithm One should be integers near $Q = M/3$ and $R_k = N/3$ [26]. Using these substitutions and further approximations we arrive the following estimate for the total flop count

$$fc_{One} \approx \tfrac{1}{3} M^3N + \tfrac{1}{2} KN^3. \quad (32)$$

Note that the K estimations of Steps 3 and 4 are independent of each other and can thus be done in parallel.

2) Operation Count for Algorithm Two

Since Algorithm Two first utilizes the first three steps of Algorithm One we obtain $fc^1_{Two} = fc^1_{One}$, $fc^2_{Two} = fc^2_{One}$, and $fc^3_{Two} = fc^3_{One}$ for the flop counts of those steps. For Steps 4–6, the roles of M and N are reversed, and Q^t and $R^t_{k'}$ are used instead of Q and R_k. We thus obtain the following for their flop counts

$$\begin{aligned} fc^4_{Two} &\approx 4M(N - Q^t)(Q^t + 1)^2 + 8(Q^t + 1)^3 \\ fc^5_{Two} &\approx 2NQ^{t2} - \tfrac{2}{3} Q^{t3} \\ fc^6_{Two} &\approx \sum_{k'=1}^{K^t} (4(M - R^t_{k'})(R^t_{k'} + 1)^2 + 8(R^t_{k'} + 1)^3). \end{aligned} \quad (33)$$

Each distance ($\Delta(\cdot, \cdot)$) calculation requires 16 flops. Thus, the flop count for Step 7 is given by

$$fc^7_{Two} = 16 \sum_{k=1}^{K} L_k \sum_{k'=1}^{K^t} L^k_{k'}. \quad (34)$$

For the QR decomposition in Step 8 the approximate flop count is given by

$$fc^8_{Two} \approx 2MN\Gamma^2 - \tfrac{2}{3} \Gamma^3. \quad (35)$$

The flop count for the SVD's, QR decompositions, and matching of Algorithm Two is given by the sum of the individual flop counts above.

Again, to achieve near optimal performance (with respect to the CRB), the model order used for Steps 1, 3, 4, and 6 of Algorithm Two should be integers near $Q = R^t_{k'} = M/3$, $R_k = Q^t = N/3$ [26]. Using these substitutions and further approximations we arrive at the following estimate for the total flop count

$$fc_{Two} \approx \tfrac{1}{3} M^3N + \tfrac{1}{2} KN^3 + \tfrac{1}{3} N^3M + \tfrac{1}{2} K^tM^3 + 2MN\Gamma^2 - \tfrac{2}{3} \Gamma^3. \quad (36)$$

Note that the number of flops required for Step 7 is negligible when compared to the other steps. Also note that the K estimations of Step 3 are independent and the K^t estimations of Step 6 are independent and can thus be done in parallel. Comparing (32) and (36), we see that for $M = N$, Algorithm Two requires about twice the computations as Algorithm One does.

3) Alternative Method for x-pole Estimation

The solution for $\hat{b}$ using (5) can become computationally intensive for large data sets. For example, in $M = N = 64$ and $Q = 20$, then S is of dimension (2816×21). Since only the right singular vectors and the singular values are needed, one can instead obtain $\hat{b}$ from a related eigendecomposition problem. Consider S^HS,

$$S^HS = \begin{bmatrix} s_1^Hs_1 & s_1^HS_2 \\ S_2^Hs_1 & S_2^HS_2 \end{bmatrix}, \quad (37)$$

where s_1 is the first column of S and S_2 are the remaining Q columns (i.e., $S = [s_1 \quad S_2]$). Note that for typical problems S contains many more rows than columns, so S^HS is smaller than S. An eigendecomposition of S^HS is performed, and all but the K largest eigenvalues are truncated to give $\widehat{S^HS}$. Finally, the minimum norm estimate of $\hat{b}$ is given by,

$$\hat{b} = -\widehat{(S_2^HS_2)}^+ \widehat{S_2^Hs_1} \quad (38)$$

where $\widehat{S_2^HS_2}$ and $\widehat{S_2^Hs_1}$ are the lower right and lower left submatrices of $\widehat{S^HS}$, respectively (37).

We note that this procedure is less numerically accurate than the previous procedure because of the squaring of the data (which occurs in S^HS) so extended precision should be used in the computations.

III. Simulations

Below we present numerical simulations to assess model validity and noise effects. Three examples are presented. The first example considers the estimation of three 2-D undamped exponentials; this example was also considered in [18]. The second example considers the estimation of three 2-D damped exponentials. The third example utilizes electromagnetic scattering data from a thin metal plate.

A. Example 1

In this example, we compare the variances of frequency estimates to their CRB's at various signal to noise ratios (SNR's) for the three 2-D frequency scenario presented in [18] using Algorithm One and Algorithm Two. Data was generated using the model in (2) for $M = N = 20$ and

$$[p_{x1} \quad p_{y1,1} \quad a_{1,1}] = [e^{j2\pi 0.24} \quad e^{j2\pi 0.24} \quad 1]$$

$$[p_{x1} \quad p_{y1,2} \quad a_{1,2}] = [e^{j2\pi 0.24} \quad e^{j2\pi 0.26} \quad 1]$$

$$[p_{x2} \quad p_{y2,1} \quad a_{2,1}] = [e^{j2\pi 0.26} \quad e^{j2\pi 0.24} \quad 1]. \qquad (39)$$

We can see that from the angles of the above poles the corresponding frequencies are 0.24 and 0.26. For the purposes of identification we will label the (x-pole, y-pole) pairs above with frequencies (0.24, 0.24), (0.24, 0.26), and (0.26, 0.24) as 2-D frequencies f_1^{2D}, f_2^{2D}, and f_3^{2D}, respectively. Note that these frequencies are spaced at four-tenths of a Fourier bin in both directions (1 Fourier bin = (1/20) = 0.05). Also note that this data consists of undamped exponentials.

The plots in Fig. 1 show the simulation results for the x-pole and y-pole frequencies, where Algorithm One was used. One hundred different noise realizations were run for each integer SNR between 0 and 50 dB. The SNR is defined as the total signal power divided by the total noise power. Specifically these figures show the estimated frequency variances for the various SNR's (they are given by the dashed lines as indicated). The corresponding CRB's are given by the solid lines; the CRB's of the model were found using the expressions in [27]. The algorithm parameters were set at $Q = 8$, $K = 2$, $R_1 = R_2 = 8$, $L_1 = L_2 = 2$ for this example. Note that we have used $Q \approx M/3$ and $R_k \approx N/3$ because these values give maximum parameter accuracy in the SVD estimation step [26].

From Fig. 1(a) we can see that the threshold SNR is 15 dB in this case. For SNR's above 15 dB, the variances are within about 4 dB of the CRB; below 15 dB the algorithm fails to reliably resolve the frequencies. The simulation variance lines cross the CRB lines at low SNR because the pole estimates cannot be reliably assigned to the true poles. Theoretically, the variance curves for f_1^{2D} and f_2^{2D} are identical; however, the variance curves from the Monte Carlo simulations separate at the lower SNR's due to differences in the y-pole estimates which cause some outliers to not be included in the variance calculations. This example was also considered in [18] for an SNR per pole of 10 dB, which corresponds to a total SNR of 17.7 dB used here. In comparison, the estimation scheme in [18] gives x-pole frequency variances which are about 3 or 4 dB better for f_1^{2D} and f_3^{2D} and about 8 dB better for f_2^{2D}.

Fig. 1(b) is a plot of the inverses of the y-pole frequency variances for the various SNR's along with the corresponding CRB's as before. From this figure we can see that the curve for the y-pole variance for f_3^{2D} exhibits the same properties as those discussed for the x-pole frequency variances above. We can see that the y-pole frequency variances for f_1^{2D} and f_2^{2D} are about 13 and 10 dB away from their respective CRB lines. We can also see that the y-pole estimation for f_1^{2D} and f_2^{2D} breaks down at SNR's below 25 dB. The fact that these variances are farther away from their CRB's and that the resolution threshold is higher is expected because of the accumulation of error which occurs in the y-pole estimates in Algorithm One. This accumulation of error does not occur in Algorithm Two, as shown below.

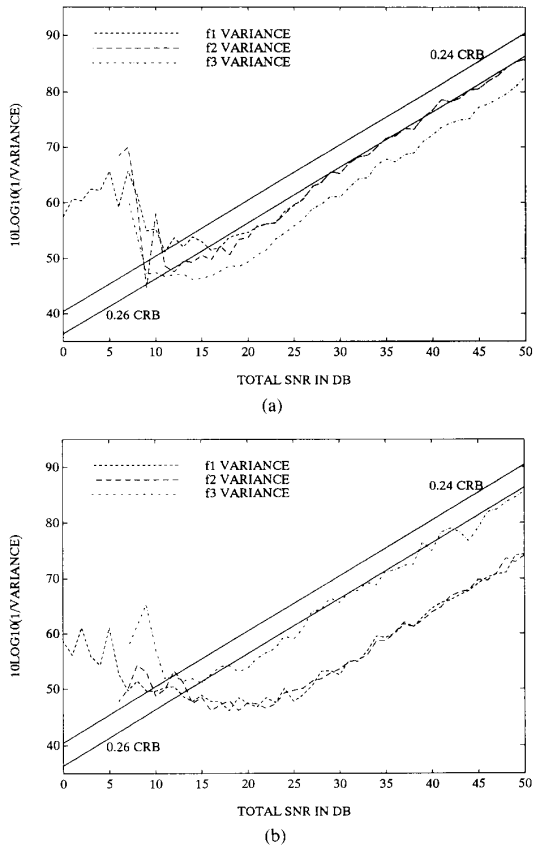

Fig. 1. Example 1. 10 $\log_{10}$ (1/Variance) versus total SNR in dB for (a) x-pole and (b) y-pole frequencies using Algorithm One.

The plots in Fig. 2 show the estimated x-pole and y-pole frequency variances for this example when Algorithm Two is used. As expected, the x-pole frequency variances are much the same as those for Fig. 1(a), but the y-pole frequency variances have been improved to match the x-pole frequency variance performance. The estimation scheme in [18] gives variances which are about 3 or 4 dB better for the y-pole frequencies of f_1^{2D} and f_2^{2D} and variances which are about 8 dB better for the y-pole frequency of f_3^{2D}.

We next consider the SVD operation counts for this example for Algorithm Two. The SVD steps are major computational parts. Each noise realization required SVD's of two 240 × 9 matrices and four 9 × 11 matrices where only the singular values and right singular vectors were

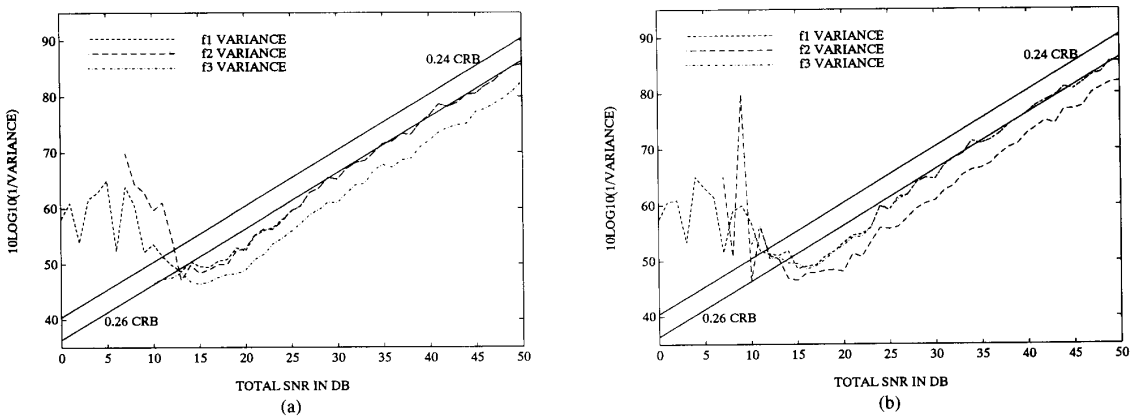

Fig. 2. Example 1. 10 $\log_{10}$ (1/Variance) versus total SNR in dB for (a) x-pole and (b) y-pole frequencies using Algorithm Two.

computed. For the same example, the algorithm in [18] required SVD's of two 49 × 169 matrices for each noise realization where the singular values and left singular vectors are computed. Looking at expressions in [25] for SVD computations we can see that Algorithm Two requires about 228 Kflops for the SVD's, whereas the algorithm in [18] requires about 5.13 Mflops for its SVD's. Thus, Algorithm Two provides a significant savings over the algorithm in [18]. We note that the SVD's for both algorithms can be performed with fewer computations by computing the eigendecomposition of smaller square matrices (37) as discussed above, with a corresponding loss in numerical accuracy. Using this idea the total number of computations are reduced for both methods, however there is still savings with Algorithm Two over the algorithm in [18].

B. Example 2

In this example we examine the estimation of damped exponentials in noise utilizing Algorithm Two. Data was generated using the model in (2) for $M = N = 20$ and

$$\begin{aligned}
[p_{x_1} \quad p_{y_{1,1}} \quad a_{1,1}] &= [0.92\,e^{j2\pi 0.24} \quad 0.92\,e^{j2\pi 0.24} \quad 3.185] \\
[p_{x_1} \quad p_{y_{1,2}} \quad a_{1,2}] &= [0.92\,e^{j2\pi 0.24} \quad 0.95\,e^{j2\pi 0.26} \quad 2.846] \\
[p_{x_2} \quad p_{y_{2,1}} \quad a_{2,1}] &= [0.95\,e^{j2\pi 0.26} \quad 0.92\,e^{j2\pi 0.24} \quad 2.846].
\end{aligned} \tag{40}$$

For the purposes of identification we will label the (x-pole, y-pole) pairs above with frequencies (0.24, 0.24), and (0.24, 0.26), and (0.26, 0.24) as 2-D pole pairs p_1^d, p_2^d, and p_3^d, respectively. The amplitude coefficients are chosen so that the energy of each mode is identical to the corresponding mode energy in Example 1.

The plots in Fig. 3 show the simulation results for the x-pole and y-pole frequency and magnitude variances. As we can see the results are similar to the undamped results in Example 1 using Algorithm Two. The variances track the CRB's as before, with the exception being that the resolution threshold is at an SNR of about 20 dB rather than 15 dB.

These results show that the algorithm is capable of estimating damped as well as undamped exponentials. In many applications such as the electromagnetic scattering problem, there are modes present whose frequency dependence are not always constant [28], which thus require damped modes as well as undamped modes. Thus the algorithm's ability to also estimate damped modes is important, as seen in Example 3 below.

C. Example 3

In this example we consider the application of Algorithm Two to the extraction of electromagnetic scattering features from a thin metal plate. A thin, 0.5 × 0.5 meter perfectly conducting square plate is fixed in space as shown in Fig. 4. Farfield monostatic 2-D scattering measurements of the plate (at horizontal transmit and receive polarization) were predicted using the geometric theory diffraction (GTD) scattering prediction method described in [28]. The scattering data were generated for frequencies of 9 to 11.55 GHz in 85 MHz steps, and for azimuth angles between $37.5° < \phi < 52.5°$ in 0.5° steps with θ fixed at 90°, for a 31 × 31 data grid. Note that the data was collected on a polar grid, not a rectangular grid; nonetheless, we assume a rectangular grid in the data processing.

Algorithm Two is applied to this data with the parameters set at $Q = R = Q^t = R^t = 10$, $K = K^t = 4$, and $L = L^t = 1$. With no noise added to the original data, the estimated parameters are

$$\begin{aligned}
[\rho_{x_1} \quad \rho_{y_1} \quad \alpha_1] &= [0.990e^{j2\pi 0.169} \quad 0.990e^{j2\pi 0.0333} \\
&\qquad 8.34 \times 10^{-4} e^{j2\pi 0.187}] \\
[\rho_{x_2} \quad \rho_{y_2} \quad \alpha_2] &= [0.992e^{-j2\pi 0.169} \quad 1.001e^{-j2\pi 0.031} \\
&\qquad 5.48 \times 10^{-4} e^{j2\pi 0.271}] \\
[\rho_{x_3} \quad \rho_{y_3} \quad \alpha_3] &= [0.998e^{-j2\pi 0.034} \quad 1.011e^{-j2\pi 0.177} \\
&\qquad 5.97 \times 10^{-4} e^{-j2\pi 0.275}]
\end{aligned}$$

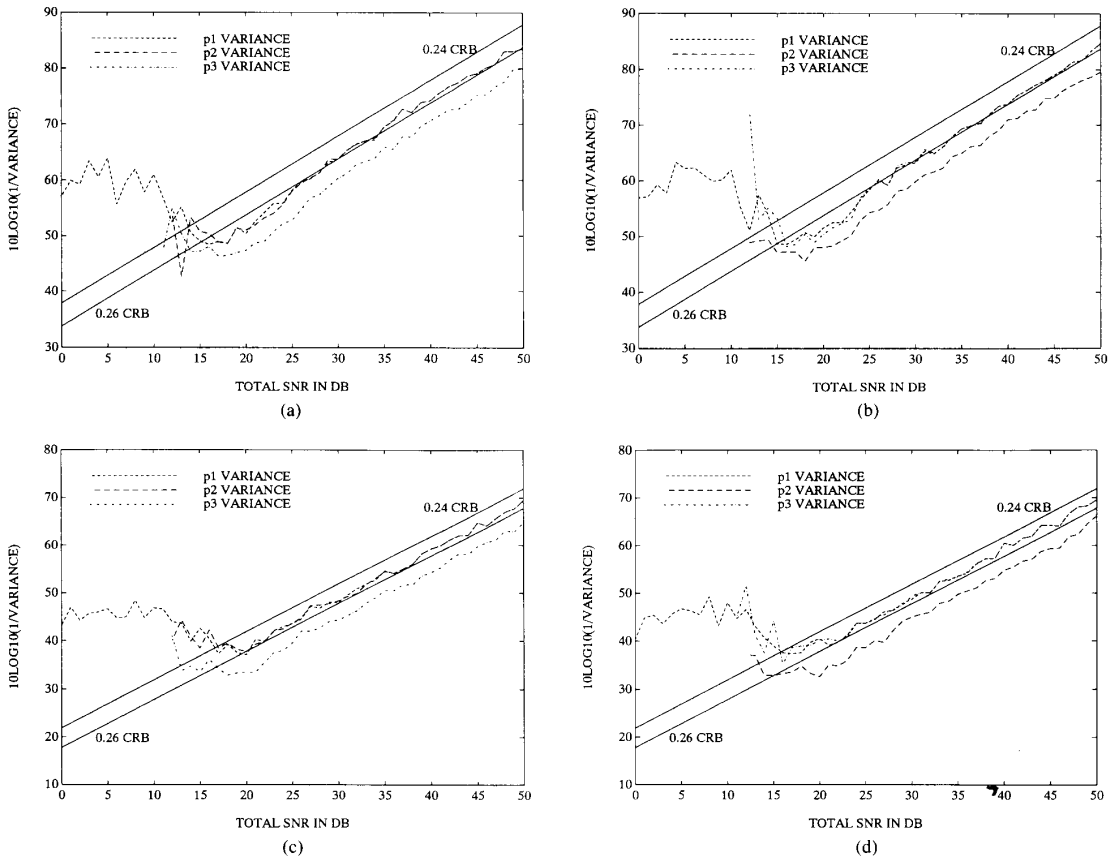

Fig. 3. Example 2. 10 $\log_{10}$ (1/Variance) versus total SNR in dB for (a) x-pole and (b) y-pole frequencies and for (c) x-pole and (d) y-pole magnitudes using Algorithm Two.

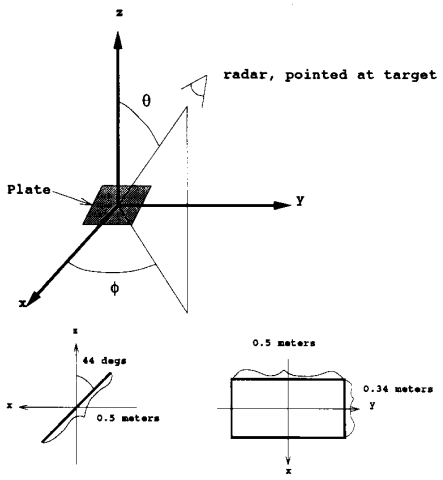

Fig. 4. Example 3. Orientation and location of thin metal perfectly conducting square plate and location of radar for scattering measurements.

$$[\rho_{x_4} \quad \rho_{y_4} \quad \alpha_4] = [1.013e^{j2\pi 0.012} \quad 0.944e^{j2\pi 0.172} \quad 2.48 \times 10^4 e^{j2\pi 0.114}] \tag{41}$$

where the units of the amplitude coefficients are volts. These four modes correspond to the tip diffraction scattering at the four corners of the plate. These modes are plotted as '○'s in Fig. 5. Fig. 5 also shows as outline of the flat plate at the middle of the rotation ($\phi = 45°$, $\theta = 90°$). The circles do not lie directly on the plate corners due to modeling errors which are present [namely, that the data are collected on a polar grid but processed assuming a rectangular grid, and that the scattering from a plate is only approximately represented by the model in (2)]. Note that these modes are damped rather than undamped, which results because the tip scattering terms depend both on frequency and angle.

Fig. 5 also shows the results of applying Algorithm Two on the GTD data. This figure shows one hundred overlapped pole estimates each with a total SNR of 20 dB and each using $Q = R = Q' = R' = 10$, $K = K' = 4$, and $L = L' = 1$. Each estimated pole is plotted as a '+' on the figure. It can be seen that these estimates are in close agreement with the noiseless pole locations (the '○' locations in the figure). It can be seen that for all the estimates, Algorithm Two correctly estimates the locations of the four scattering terms at the four corners of the plate. This example shows the utility of Algorithm Two when applied to electromagnetic scattering data.

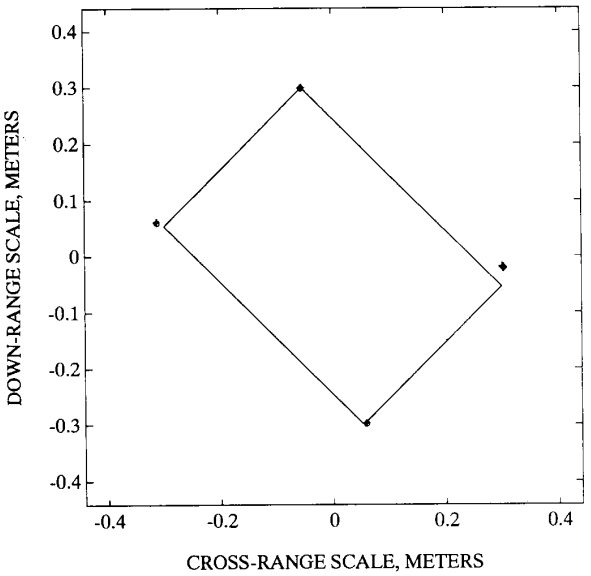

Fig. 5. Example 3. Scatter plots of pole locations in the range domain for a total SNR of 20 dB. Estimated pole locations are denoted by "+." Noiseless pole locations are denoted by "○."

IV. Conclusions

We have presented a new method for estimating 2-D exponential modes and amplitude coefficients. This method utilizes a 1-D TLS-based Prony model and estimation technique. This process has computational advantages over methods which have independent steps such as the one in [18] since the second step involves several smaller estimations rather than one estimation as large as the first. This procedure also has the advantage not requiring a pairing of x and y-poles.

Simulations demonstrate the algorithms ability to estimate 2-D pole pairs and amplitude coefficients in the presence of noise reasonably well. The estimates in [18] are slightly more accurate than the estimates for this technique, but this technique offers computational savings over the one in [18]. For Algorithm One, the y-pole estimation is less accurate than the x-pole estimation due to a propagation of error in the x-pole estimation. If more accuracy is required in both the x and y-pole estimates then Algorithm Two can be implemented which and this has computational savings over [18].

References

[1] P. M. Joseph and R. D. Spital, "The exponential edge-gradient effect in X-ray computed tomography," *Phys. Med. Biol.*, pp. 473-487, 1981.
R. M. Lewitt, "Reconstruction algorithms: Transform methods," *Proc. IEEE*, vol. 71, pp. 390-408, Mar. 1983.
[3] Y. Censor, "Finite series-expansion reconstruction methods," *Proc. IEEE*, vol. 71, pp. 409-419, Mar. 1983.
[4] D. J. Rossi and A. S. Willsky, "Reconstruction from projections based on detection and estimation of objects—parts I and II: Performance analysis and robustness analysis," *IEEE Trans. Acoust., Speech, Signal Processing*, vol. SP-32, Aug. 1984.
[5] G. M. Dural, "Polarimetric ISAR imaging to identify basic scattering mechanisms using transient signatures," Ph.D. dissertation, Ohio State Univ., Columbus, OH, Dec. 1988; also in ElectroScience Lab. Rep. 312884-9.
[6] S. M. Scarborough, "Ultrawideband radar imaging and the diagnosis of scattering centers," M.S. thesis, Ohio State Univ., Columbus, OH, 1990.
[7] L. M. Novak, "A comparison of 1-D and 2-D algorithms for radar target classification," in *IEEE Int. Conf. on Syst. Eng.*, Dayton, OH, Aug. 1-3, 1991, pp. 6-12.
[8] J. Capon, "High resolution frequency-wavenumber spectrum analysis," *Proc. IEEE*, vol. 57, pp. 1408-1418, Aug. 1969.
[9] J. A. Cadzow and K. Ogino, "Two-dimensional spectral estimation," *IEEE Trans. Acoust., Speech, Signal Processing*, vol. ASSP-29, pp. 396-401, June 1981.
[10] J. S. Lim and N. A. Malik, "A new algorithm for two-dimensional maximum entropy power spectrum estimation," *IEEE Trans. Acoust., Speech, Signal Processing*, vol. ASSP-29, pp. 401-413, June 1981.
[11] J. H. McClellan, "Multidimensional spectral estimation," *Proc. IEEE*, vol. 70, pp. 1029-1039, Sept. 1982.
[12] S. M. Kay, *Modern Spectral Estimation, Theory and Application.* Englewood Cliffs, NJ: Prentice-Hall, 1988.
[13] B. F. McGuffin and B. Liu, "An efficient algorithm for two-dimensional autoregressive spectrum estimation," *IEEE Trans. Acoust., Speech, Signal Processing*, vol. 37, pp. 106-117, Jan. 1989.
[14] A. J. Devaney and G. A. Tsihrintzis, "Maximum likelihood estimation of object location in diffraction tomography," *IEEE Trans. Acoust., Speech, Signal Processing*, vol.39, pp. 2004-2005, Mar. 1991.
[15] N. J. Dusaussoy and I. E. Abdou, "The extended MENT algorithm: A maximum entropy type algorithm using prior knowledge for computerized tomography," *IEEE Trans. Acoust., Speech, Signal Processing*, vol. SP-39, pp. 1164-1180, May 1991.
[16] S. W. Lang and J. H. McClellan, "Multidimensional mem spectral estimation," *IEEE Trans. Acoust., Speech, Signal Processing*, vol. ASSP-30, pp.880-887, Dec. 1982.
[17] S. Y. Kung, K. S. Arun, and D. V. B. Rao, "State-space and singular-value decomposition-based approximation methods for the harmonic retrieval problem," *J. Opt. Soc. Am.*, vol. 73, pp. 1799-1811, Dec.1983.
[18] Y. Hua, "Estimating two-dimensional frequencies by matrix enhancement and matrix pencil," in *Proc. of the Int. Conf. on Acoust., Speech, and Signal Processing*, Toronto, ON, May 14-17, 1991, pp. 3073-3076.
[19] M. A. Rahman and K.-B. Yu, "Total least squares approach for frequency estimation using linear prediction," *IEEE Trans. Acoust., Speech*, Signal Processing, vol. ASSP-35, pp. 1440-1454, Oct. 1987.
[20] T. J. Abatzoglou and L. K. Lam, "Direction finding using uniform arrays and the constrained total least squares method," in *Proc. of the 25th Asilomar Conf. on Signals, Systems, and Computers*, Pacific Grove, CA, November 4-6, 1991.
[21] J. J. Sacchini, "Development of two-dimensional parametric radar signal modeling and estimation techniques with application to target identification," Ph.D. dissertation, Ohio State Univ., Columbus, OH, Mar. 1992.
[22] Y. T. Chan and R. P. Langford, "Spectral estimation via the high-order Yule-Walker equations," *IEEE Trans. Acoust., Speech, and Signal Processing*, vol. ASSP-30, pp. 689-698, Oct. 1982.
[23] J. A. Cadzow, "Spectrum estimation: An overdetermined rational model equation approach," *Proc. IEEE*, vol. 70, pp. 907-939, Sept. 1982.
[24] P. Stoica, T. Söderström, and F. Ti, "Asymptotic properties of the high-order Yule-Walker estimates of sinusoidal frequencies," *IEEE Trans. Acoust., Speech, Signal Processing*, vol. 37, pp. 1721-1734, Nov. 1989.
[25] G. H. Golub and C. F. V. Loan, *Matrix Computations*—2nd ed. Baltimore: Johns Hopkins Univ. Press, 1989.
[26] Y. Hua and T. K. Sarkar, "A perturbation property of the TLS-LP method," *IEEE Trans. Acoust., Speech, Signal Processing*, vol. 38, pp. 2004-2005, Nov. 1990.
[27] W. M. Steedly and R. L. Moses, "The Cramér-Rao bound for pole and amplitude estimates of damped exponential signals in noise," in *Proc. of the Int. Conf. on Acoust., Speech, and Signal Processing*, Toronto, ON, May 14-17, 1991, pp. 3569-3572.
[28] R. J. Marhefka, "Radar cross section-basic scattering code rcs-bsc (version 2.0) user's manual," *Dep. Elec. Eng.*, ElectroScience Laboratory, Ohio State Univ., Columbus, OH, Tech. Rep. 718295-15, Feb. 1990.

Joseph J. Sacchini (S'83-M'84-S'88-M'93) received the B.E. degree from Youngstown State University, Youngstown, OH, in 1984, the M.S. degree in electrical engineering from the University of Dayton, Dayton, OH, in 1988, and the Ph.D. degree in electrical engineering from Ohio State University, Columbus, OH, in 1992. He received his officer commission in United States Air Force in 1984 and is now a Captain.

From 1984 to 1988, he worked extensively on electronic warfare systems on various operational aircraft. He is currently an Assistant Professor at the Air Force Institute of Technology. His primary research interests are in parametric signal processing, radar target identification, communication theory, and digital communication.

Dr. Sacchini is a member of Tau Beta Pi, Phi Kappa Phi, NSPE, and is registered in Ohio as a professional engineer.

William M. Steedly (S'86-M'93), for a photograph and biography, see p. 1318 of the March 1993 issue of this TRANSACTIONS.

Randolph L. Moses (S'83-M'84-SM'90), for a photograph and biography, see p. 1318 of March 1993 of this TRANSACTIONS.